

# Dark resonances as a probe for the motional state of a single ion

C. Lisowski, M. Knoop,\* C. Champenois, G. Hagel, M. Vedel, and F. Vedel

*Physique des Interactions Ioniques et Moléculaires (CNRS UMR 6633),  
Université de Provence, Centre de Saint Jérôme, Case C21, 13397 Marseille Cedex 20, France*

(Dated: Received: January 4, 2020/ Revised version: date)

Single, rf-trapped ions find various applications ranging from metrology to quantum computation. High-resolution interrogation of an extremely weak transition under best observation conditions requires an ion almost at rest. To avoid line-broadening effects such as the second order Doppler effect or rf heating in the absence of laser cooling, excess micromotion has to be eliminated as far as possible. In this work the motional state of a confined three-level ion is probed, taking advantage of the high sensitivity of observed dark resonances to the trapped ion's velocity. Excess micromotion is controlled by monitoring the dark resonance contrast with varying laser beam geometry. The influence of different parameters such as the cooling laser intensity has been investigated experimentally and numerically.

PACS numbers: 32.80.Pj, 39.30.+w

## I. INTRODUCTION

Dark resonances in a three-level system, also called coherent population trapping, are a well-known example of destructive quantum interference based on the interaction of two light fields generating the coherent superposition of two atomic states. Various applications of the coherent population trapping scheme can be found in atomic physics from high-resolution spectroscopy to sub-recoil laser-cooling of an atom cloud [1] or EIT-cooling of single ions [2, 3]. Dark resonances have been readily observed in trapped ions, almost exclusively with copropagating laser beams [4, 5, 6, 7]. In general the observed splitting of the various Zeeman levels is used for an exact quantitative calibration of the local magnetic field.

Single ions confined in radiofrequency traps are ideal candidates for different applications of high-resolution spectroscopy such as quantum information or frequency standards in the optical domain [8]. They can be stored in the trap from hours up to months in a quasi interaction-free environment, oscillating at fixed frequencies in an effective pseudo-potential well. Laser cooling of a single trapped ion allows to reach the Doppler cooling limit which is in the mK-range. To eliminate residual Doppler broadening on a given transition, the ion's excursion along the laser propagation direction must be smaller than the inverse wavenumber to fulfill the Lamb-Dicke condition [9]. The excitation spectrum of the considered transition is then decomposed in a central carrier and a few sidebands separated by the ion's frequencies of motion (Lamb-Dicke regime).

The excellent spatial localisation required by the Lamb-Dicke condition can only be achieved in the low-field region of the rf trapping field. Experimentally, this is realized with the confinement of single ions in the potential minimum of the trap, with one exception where two ions have been stored in an extraordinarily steep, elliptical potential [10]. For this purpose, the pseudo-potential at the position of the ion has to be nearly perfectly symmetric. Flaws in the potential due to asymmetries or patch potentials caused by atom deposition during ion creation, may distort the created potential and deviate the minimum of the trap's AC electric field from the minimum of the pseudo-potential well. The resulting displacement of the average position of the ion in the trap causes an increase of the velocity amplitude at the confinement frequency, called excess micromotion, and has to be corrected. The influence of parasitic potentials can be compensated by direct voltages applied on supplementary correction electrodes in the vicinity of the trap.

Different experimental techniques have been employed to reduce the excess micromotion of a single trapped ion ([11] and references therein). In this paper we present an additional and straightforward method for the localisation of an ion in the miniature trap. We have used coherent population trapping as a tool to minimize the micromotion of the confined ion. Dark resonances depend ideally only on the lifetimes of the two involved atomic states, which in the present experiment are the  $4S_{1/2}$  ground state and the metastable  $3D_{3/2}$  state (natural lifetime close to 1 s [12, 13]) of a single calcium ion confined in a miniature cylindrical ring trap. In practice, the lifetime of the dark state is shortened by the linewidth of the lasers, leading to a reduction of the visibility of the dark resonance. The oscillating

---

\*Electronic address: Martina.Knoop@up.univ-mrs.fr

Doppler shifts encountered by the ion also tend to wash out the dark resonance, if the dark state is not stable on the observation time scale. The study of the phenomenon reveals that the maximum sensitivity to the velocity amplitude of the ion is reached with counterpropagating laser beams. The proposed technique is based on the fact that the depth of dark resonances observed in the fluorescence of a single ion increases with the degree of immobilisation of the ion. Excess micromotion drastically reduces the lifetime of the dark state, smoothing the observed dark resonance dip.

The first section of this article describes the micromotion generated in the radiofrequency trap, the existing methods to reduce this effect are very briefly reviewed. We then introduce the formalism for dark resonances, along with the modelling used to obtain a high degree of control of the experimental conditions. The subsequent section presents numerical results, while the last section of this work is devoted to the experimental observation of dark resonances and its use as a tool to reduce excess micromotion. The influence of the main control parameters (laser power, beam geometry and magnetic field) is discussed.

Although we try to keep our discussion of the dark resonances in a three-level system as general as possible, we use the case of a single trapped calcium ion as an illustration throughout the description of the modelling. Experimental details are given in section V, the level scheme with the relevant transitions of the calcium ion is given in figure 1.

## II. MICROMOTION IN A PAUL TRAP

The motion of a trapped ion in an ideal Paul trap is described by the Mathieu equations [14]:

$$\frac{d^2u}{d\tau^2} + [a_u - 2q_u \cos(2\tau)]u = 0 \quad \text{with} \quad \tau = \frac{\Omega}{2}t \quad (1)$$

valid for the three directions  $u = x, y, z$ . The values of the coefficients  $a_u$  and  $q_u$  which determine the range of stable confinement of a particle are defined by the trapping voltage  $V_{AC}$  and its frequency  $\Omega/2\pi$ , the superimposed DC-voltage  $V_{DC}$ , the radius  $r_0$  of the trap as well as the  $e/m$  ratio of the trapped ion. To first order in  $a_u$  and  $q_u$ , the stable solution of equation (1) is

$$u(t) = R_u \cos \omega_u t \left(1 + \frac{q_u}{2} \cos \Omega t\right) \quad (2)$$

The motion of the confined ion is composed of the harmonic oscillation at frequencies  $\omega_u/2\pi$  with amplitude  $R_u$  called "secular" motion, and the AC-driven "micromotion" at the frequency of the trapping field  $\Omega/2\pi$ . In opposition to the secular motion, micromotion cannot be cooled because it is driven motion. According to Eq.(2), a smaller secular motion amplitude  $R_u$  leads to a reduced contribution of the micromotion. A displacement  $D_u$  of the average position of the ion, due to asymmetries in the geometry of the trap and the applied electric fields, causes excess micromotion, and can be taken into account like

$$u(t) = (R_u \cos \omega_u t + D_u) \left(1 + \frac{q_u}{2} \cos \Omega t\right) \quad (3)$$

in the equation of motion. This excess micromotion can possibly prevent the access to the Lamb-Dicke regime. A complete review of origin and consequences of the micromotion is given in [11].

Three experimental methods allow to control excess micromotion of an ion in a radiofrequency trap. Best results are obtained by using all of them as the collected information is complementary in the three cases. The control parameter is in either case the set of DC-voltages applied to the compensation electrodes surrounding the trap. The most simple approach is the observation of the spatial displacement of a trapped ion as the confining potential is lowered. Parasite potentials then gain in importance and move the ion out of the trap center. This method requires spatial detection of the ion's fluorescence and is limited to the plane of observation. Another means for the rejection of excess micromotion is to probe the fluorescence linewidth of the laser-cooling transition. When the blue laser is scanned, only the low-frequency side of the atomic resonance is experimentally visible, as the high-frequency detunings induce a Doppler laser heating effect, causing a sudden drop in fluorescence signal. This profile is difficult to calibrate in terms of absolute temperature, but gives a good relative control signal of the ion's kinetic energy when laser powers are fixed. At a given laser frequency, the half-maximum fluorescence signal decreases for better compensation, as the ion becomes colder and its blue transition linewidth narrower. A more specific observation of the micromotion's influence is the measure of the correlation of the emitted fluorescence photons with the confinement frequency  $\Omega/2\pi$  [11]. Actually, the oscillatory motion of the ion causes a frequency modulation of the laser field in the rest frame of the ion, and induces a modulation of the emitted photons at the trapping frequency  $\Omega/2\pi$ . To cancel the micromotion, the amplitude of this modulation signal has to be minimized. Best compensation results are obtained by the use of different laser axes for an access to the different projections in space.

The ultimate measurement to determine the absolute degree of localisation of the ion in the trap is the detection of vibrational sidebands in the excitation spectrum of the ion. The trapped ion oscillates at secular frequencies  $\omega_u/2\pi$  and at the confinement frequency  $\Omega/2\pi$ . The oscillatory motion at a fixed frequency creates a frequency modulation of the laser excitation through the oscillating Doppler effect and leads to sidebands in the excitation spectrum. The relative height of the sidebands is related to the amplitude of the corresponding oscillation, and their minimization is thus an indicator for the localization of the ion [15]. Sideband observation in the excitation spectrum is only possible on a transition whose natural linewidth is inferior to the ion's vibrational frequencies. In the present experiment, it must be realized on the ultra-narrow  $4S_{1/2} - 3D_{5/2}$  transition using the quantum jump technique. The experimental realization requires a highly stabilized laser to excite the  $4S - 3D$  transition and the need to work on quantum jump statistics for the detection of this dipole-forbidden transition.

In the following we show how the visibility of the dark resonance varies with experimental conditions and how we can use this observation to probe the minimisation of the micromotion of the confined particle.

### III. FORMALISM AND MODELLING

In a three-level system driven by two lasers in  $\Lambda$  configuration, coherent superposition of the atomic states coupled by the radiation fields leads to the appearance of a non-absorbing state, when the detunings of the two lasers are equal. In this case, one of the stationary states  $|\psi_{NC}\rangle$  is a coherent superposition of the ground and metastable states  $S_{1/2}$  and  $D_{3/2}$ , which is not coupled to the excited state  $P_{1/2}$  by the atom-laser interaction  $V_L$  ( $\langle P_{1/2} | V_L | \psi_{NC} \rangle = 0$ ). Once in this state, the atom can neither absorb nor scatter photons and the fluorescence disappears. This feature, called dark resonance, has been used to cool atoms below the recoil limit by velocity selective coherent population trapping [16], and ions to the vibrational ground state by electromagnetically induced transparency [2].

In the general case, the two transitions are driven by different lasers, the non-coupled state then depends on the relative phase of the lasers, labelled (B) and (R) for blue and red, like:

$$|\psi_{NC}\rangle = e^{-i(\omega_B t + \phi_B)} \frac{-\Omega_B |D_{3/2}\rangle + \Omega_R e^{-i((\omega_R - \omega_B)t + \phi_R - \phi_B)} |S_{1/2}\rangle}{\bar{\Omega}} \quad (4)$$

with  $\bar{\Omega} = \sqrt{\Omega_B^2 + \Omega_R^2}$ , where we suppose the two Rabi frequencies  $\Omega_B$  and  $\Omega_R$ , to be real. This dependance implies a high stability of the applied lasers to observe the complete extinction of the emitted fluorescence.

If the travelling wave nature of the laser fields and the motion of the atom are taken into account, the laser couples  $|P_{1/2}, p\rangle$  with  $|S_{1/2}, p - \hbar k_B\rangle$  and  $|D_{3/2}, p - \hbar k_R\rangle$ , where  $p$ ,  $\hbar k_B$  and  $\hbar k_R$  are respectively the projection of the atom momentum, the blue and the red photon momentum, along the common propagation axis of the two lasers. Then, the non coupled state is not an eigenstate of the kinetic energy and is coupled to its orthogonal state  $|\psi_C\rangle$  by the kinetic energy operator:

$$|\psi_C\rangle = \frac{\Omega_R e^{-i(\omega_R t + \phi_R)} |D_{3/2}, p - \hbar k_R\rangle + \Omega_B e^{-i(\omega_B t + \phi_B)} |S_{1/2}, p - \hbar k_B\rangle}{\bar{\Omega}} \quad (5)$$

In the basis of the atom dressed by  $N_B$  blue photons and  $N_R$  red photons, we study the evolution of the system inside the family state  $\mathcal{F}_p$  :

$$\mathcal{F}_p = \left\{ |S_{1/2}, p - \hbar k_B, N_B + 1, N_R\rangle; |P_{1/2}, p, N_B, N_R\rangle; |D_{3/2}, p - \hbar k_R, N_B, N_R + 1\rangle \right\} \quad (6)$$

The lifetime of the non-coupled state is shortened by its coupling to its orthogonal state which is

$$\langle \psi_C | H_0 + \frac{p^2}{2m} | \psi_{NC} \rangle = \frac{\Omega_B \Omega_R}{\bar{\Omega}^2} \left( \hbar(\Delta'_B - \Delta'_R) + p \frac{\hbar(k_R - k_B)}{m} \right) \quad (7)$$

where  $\Delta'_R$  and  $\Delta'_B$  are the laser detunings corrected by the photon recoil energy:  $\Delta' = \omega - \omega_{at} + \hbar^2 k^2 / 2m$ . In the case of two identical-wavelength transitions driven by copropagating laser beams ( $k_R = k_B$ ), the non coupled state is stationary as soon as the corrected detunings are equal. If the two laser beams are counterpropagating or in the more general case of different wavelengths ( $|k_R| \neq |k_B|$ ), the non-coupled state is stationary only if the atom is at rest in the excited state ( $p = 0$ ).  $(-\Omega_B |D_{3/2}, -\hbar k_R\rangle + \Omega_R |S_{1/2}, -\hbar k_B\rangle) / \bar{\Omega}$  is then a perfect trap state, as long as we neglect its finite lifetime caused by spontaneous emission. In the case of a moving atom ( $p \neq 0$ ), the dark resonance condition can be interpreted as an equality of the two detunings corrected by the Doppler shifts :

$$\Delta'_B - \Delta'_R - (k_B - k_R) p/m = 0 \quad (8)$$

It appears from equations (7) and (8) that the lifetime of the non coupled (or dark) state is reduced by the oscillating Doppler shifts as the relative laser detuning is fixed. The observation of the dark resonances can then be used to quantify the motional state of an ion, and the highest sensitivity to this motion is obtained for  $k_R = -k_B$ .

To identify the dependance of the dark resonance profile on each experimental parameter (laser linewidth, laser intensity and detuning, motional state of the ion), we numerically studied the atomic system through the evolution of its density matrix. As the number of detected photons is proportional to the population of the  $4P_{1/2}$ -level, the dark resonances are visualized by calculating this population as a function of the red laser detuning. The states involved in the simulation are the eight Zeeman sublevels of the  $S_{1/2}, P_{1/2}, D_{3/2}$  states, coupled by the blue laser (B) on the  $4S_{1/2} \rightarrow 4P_{1/2}$  transition and the red laser (R) on the  $3D_{3/2} \rightarrow 4P_{1/2}$  transition. The blue and red laser linewidths  $\Gamma_{LB}$  and  $\Gamma_{LR}$  (FWHM) are taken into account by relaxation on coherences. The mechanical effect of light on the motion of the atom is neglected as well as the recoil energy which is much smaller than the relevant energy scale of our simulations. The motion of the ion is then treated classically and taken into account by a time-dependent Doppler shift, using the same approach as in [17] :

$$\Delta_B(t) = \Delta_B^0 - k_B V(t) ; \Delta_R(t) = \Delta_R^0 \pm k_R V(t) \quad (9)$$

where the sign of the red-transition Doppler shift depends on the propagation configuration of the lasers ( $-$  for copropagating beams,  $+$  for counterpropagating beams).  $\Delta^0$  is the detuning set by the laser frequency. For the sake of simplicity, we suppose here that only one secular frequency ( $\omega_r$ ) contributes to the Doppler shift, which can be written, according to the equation of motion (3) with  $V_0 = \omega_r R_r$ :

$$\Delta(t) = \Delta^0 \pm kV_0 \left( \sin \omega_r t \left( 1 + \frac{q_r}{2} \cos \Omega t \right) + \sqrt{2} \cos \omega_r t \sin \Omega t + \frac{D_r}{R_r} \sqrt{2} \sin \Omega t \right) \quad (10)$$

using the relation  $\omega_r = q_r \Omega / (2\sqrt{2})$  valid in the adiabatic approximation [18] for a trap with zero DC field applied ( $a_r = 0$ ).

The natural widths of the involved atomic transitions are of the same order as the secular and rf trapping frequency ( $\Gamma_B/2\pi = 22.5$  MHz,  $\Gamma_R/2\pi = 1.35$  MHz,  $\omega_r/2\pi = 1$  MHz,  $\Omega/2\pi = 11.6$  MHz). For the modelling of the internal state the evolution of the density matrix has to be followed and integrated over several periods, until a steady state is reached. Technically convergence is accomplished when the level populations averaged over one secular period are not modified by adding one period to the integration time.

If the magnetic field is set to zero, the atomic population is trapped in the  $D_{3/2}, m_J = \pm 3/2$  states and fluorescence disappears and hides the dark resonance we are looking for. To prevent this optical pumping and keep the detected fluorescence signal as high as possible, a minimal magnetic field must be applied (see section V A for details).

#### IV. NUMERICAL RESULTS

Numerical simulations using the described model have been carried out to evidence the influence of the excess micromotion, the laser intensity and the laser beam geometry. To describe the dark resonance behavior in a quantitative way, we define the "contrast"  $\mathcal{C}$  of the dark resonance as the depth of the observed dip divided by the total signal we would observe at the same frequency if there was no dark resonance. This is done by numerical extrapolation of the experimental signal.

The sensitivity of the dark resonances to the excess micromotion of the ion is illustrated in figure 2 where the probability of occupation of the  $P_{1/2}$  state is plotted versus the detuning of the red laser with fixed amplitude of secular oscillation  $V_0$  and for identical laser parameters. To keep the discussion general and take advantage of the described method even for a non-ideal system, the velocity amplitude  $V_0$  is chosen to be 1 m/s which corresponds to a temperature of ten times the theoretical Doppler laser cooling limit for calcium ions. Anyway, simulations show that for the chosen laser parameters, the dark resonance can be observed up to temperatures a hundred times the Doppler cooling limit. The laser linewidths used in the simulation ( $\Gamma_{LB} = 1$  MHz,  $\Gamma_{LR} = 0.2$  MHz) are the measured linewidths of the lasers in our experiment. The Rabi frequencies ( $\Omega_B = 120$  MHz,  $\Omega_R = 30$  MHz) and the blue laser detuning ( $\Delta_B = -50$  MHz) are the highest values chosen such that the simulations reproduce the width and profile of the experimental spectra. The precision of this adjustment is of the order of 10%, which is sufficient for the comparison we want to make. As in our experiment, the magnetic field has been set to 1 Gauss. With the laser linewidths considered here, the splitting of the Zeeman sublevels can not be observed in the dark resonance.

The spectra obtained for three different displacements  $D_u$  in the counter-propagating laser beam configuration are plotted in figure 2. The depth of the dark resonance is reduced for increasing displacement and illustrates how the observation of the contrast of dark resonances can be used for the reduction of the excess micromotion. The curve

with zero excess micromotion ( $D_u = 0$ ) shows a contrast  $\mathcal{C}$  of 91%. Finite laser linewidths and secular motion prevent the dark resonance dip to fall completely to the background light level and limit the maximum contrast.

When the displacement  $D_u$  increases from 0 to 0.5 and  $1\mu\text{m}$ , the contrast is reduced to 83% and 73%, respectively. With the laser parameters given above, the blue spectral linewidths corresponding to the shown spectra do not increase, as the power broadening is too important. This means that neither the rf correlation technique nor the measurement of the spectral linewidth can give information about the reduction of the micromotion, whereas the contrast of the dark resonance can vary from 73% to 91%, which can be detected experimentally with high efficiency.

Figure 3 shows that in our experiment the observation of dark resonances can be made easier by using a higher Rabi frequency  $\Omega_B$  for the blue laser, even though the dark resonance phenomenon occurs independently of the employed Rabi frequencies. In the dressed atom picture, higher Rabi frequencies increase the splitting of the two states  $S_{1/2}$  and  $P_{1/2}$  (see inset of figure 1 for details), and thus broaden the dark resonance, making it more insensitive to the oscillating Doppler shifts. This is illustrated by figure 3 where the excitation probability to  $P_{1/2}$  is plotted for different Rabi frequencies. These examples show that  $\mathcal{C}$  has a minimum value, depending on the laser parameters  $\Omega_B$ ,  $\Omega_R$ , and  $\Delta_B$ , even if the dark resonance gets washed out by the oscillating Doppler shifts. In the cases studied in figure 3, the contrast is 53% for  $\Omega_B = 60$  MHz and increases to 83% for  $\Omega_B = 120$  MHz. In return, micromotion sidebands, which are visible as an additional structure in the spectrum calculated for  $\Omega_B$  are smoothed by power broadening for  $2\Omega_B$ . This dependence on the Rabi frequencies implies that the use of the dark resonance contrast for the reduction of the displacement  $D_u$  has to be made at constant laser power.

## V. EXPERIMENTAL RESULTS

We trap singly-ionized calcium in a miniature cylindrical radiofrequency trap. The main laser-cooling transition connects the  $4S_{1/2}$  ground state to the  $4P_{1/2}$ -level at 397 nm (called the blue transition (B)), shown on the inset of figure 1. This upper state has a lifetime of 7 ns and a branching ratio to the metastable  $3D_{3/2}$ -state of about 6%. A closed laser-cooling cycle therefore requires a repumper laser at 866 nm (red transition (R)) to empty the  $3D_{3/2}$ -state. Our experimental set-up is based on a miniature ring trap with an inner diameter of 1.4 mm. The trapping frequency of  $\Omega/2\pi \simeq 11.6$  MHz with an amplitude of about  $V_{AC} = 300$  V is applied to the ring, generating a pseudo-potential well with a depth of a few eV, allowing the confinement of ions for very long periods. Two tip electrodes in the plane of the ring ( $x, y$ ) and two larger mesh electrodes along the ring axis ( $z_1, z_2$ ), distant by approximately 5 mm from the ring center, permit corrections of the potential by application of direct voltages. The trapping characteristics of this device are described in detail elsewhere [19].

The experimental geometry is like in [20] and in figure 1, where the case of counterpropagating laser beams is depicted. The ultrahigh-vacuum vessel containing the miniature trap allows the propagation of the laser beams along an axis having a 55 degree angle according to the trap's  $z$ -axis. The ion's fluorescence is observed in the  $xy$ -plane of the trap either spatially resolved by an intensified CCD or as an integrated signal by a photomultiplier in photon-counting mode. Laser beams are transported to the trap by single-mode fibers, polarization-maintaining in the case of the blue laser. Laser polarizations are modified by means of quarter- and half-waveplates.

Since dark resonances require identical detuning for both lasers, their observation can be readily realized by keeping one laser fixed, while probing the atomic resonance by scanning the other laser. In order to observe a full fluorescence spectrum without losing the ion by Doppler laser heating, the blue cooling laser is fixed on the red-frequency side of the  $4S_{1/2}$ - $4P_{1/2}$  transition (approximately at - 1 to - 2  $\Gamma_B$ ) and the frequency of the repumper laser at 866 nm is scanned. Throughout the experiments presented in this section, the laser beam geometry has been chosen to be counter-propagating, except for figure 8.

An experimentally recorded dark resonance signal as well as its corresponding numerical simulation are plotted in figure 4. The excellent agreement between experiment and simulation allows to deduce the effective experimental parameters, which in this case produce lower Rabi frequencies ( $\Omega_B = 60$  MHz,  $\Omega_R = 15$  MHz) than those used in figures 2 and 3. The dashed curve on this graph is the simulation using exactly identical parameters but changing the laser geometry to copropagating beams. The dark resonance is then much more pronounced. Actually, the dependence of the computed and the observed spectra on the relative direction of propagation of the laser beams confirms the fact that the described phenomenon is indeed produced by coherent superposition.

### A. Magnetic field

To make sure that laser polarization effects do not play a role, the local magnetic field has to be controlled in a rigorous way. We apply a magnetic field sufficient to define a quantization axis but small enough to limit the splitting of the Zeeman sublevels to values lower than the natural width of the involved transition. In our experimental setup,

the local magnetic field is controlled by three pairs of orthogonal Helmholtz coils. The residual  $\vec{B}$ -field at the position of the ion has been compensated making use of an optical pumping effect. Laser-cooling is carried out on the  $4S_{1/2} - 4P_{1/2}$  transition, while a repumper on the  $3D_{3/2} - 4P_{1/2}$  transition at 866 nm avoids trapping of the ion in the metastable  $3D_{3/2}$  state. A bias magnetic field  $\vec{B}_0$  ( $\approx 1$  Gauss) is applied perpendicularly to the propagation axis of the lasers, the repumping laser being linearly polarized parallel to this field. If the total magnetic field is parallel to  $\vec{B}_0$ , the ion is pumped in the  $3D_{3/2}$ ,  $m_J = \pm 3/2$  states, which are not coupled to the laser, making the fluorescence disappear. Any residual magnetic field perpendicular to  $\vec{B}_0$  mixes these dark states with the  $3D_{3/2}$ ,  $m_J = \pm 1/2$  states and fluorescence is then observed again. If the repumping laser polarisation is purely linear, the observed fluorescence can be reduced to zero when the applied magnetic field exactly compensates the local field (see figure 5). This procedure is carried out for all three axis of the magnetic field, changing the quantization axis and the corresponding laser polarizations. The method, based on optical pumping in a dark state, is independent on the linewidth and detuning of the lasers, if we assume that the bias magnetic field is small enough to keep the splitting of the Zeeman sublevels comparable to the excitation linewidth of the lasers. As a consequence, this technique is not sensitive to the motion of the ion and presents the advantage of being useable for a single ion as well as for an ion cloud.

### B. Laser intensity

As discussed above higher laser intensity at 397 nm splits the atomic levels to a greater extent and increases the visibility of the dark resonance. The five graphs in figure 6 have been taken with increasing laser power, starting from 20  $\mu\text{W}$ , which corresponds to a Rabi frequency of about  $2 \Gamma_B$ , as determined from numerical adjustments. The digging of the dark resonance dip with the applied blue laser power follows a saturation curve as represented in the inset of the figure. For laser intensities higher than  $10 \Gamma_B$  the transition is largely saturated, and the maximum contrast of the dark resonance is reached.

The influence of the red probe laser intensity has also been checked while keeping the blue laser power fixed. As expected, this only broadens the scanned atomic transition, without increasing the visibility of the dark resonance, as power broadening effects prevail on the light shift effect.

### C. Micromotion

For counterpropagating laser beams, dark resonances have merely be observed in our experiment when the ion is well localized, which means that part of the excess micromotion has already been eliminated by a rough compensation of the parasite potentials. Simulations have shown the dependence of the contrast of the dark resonance on the degree of localisation of the ion (see figure 2). The smaller the ion's amplitude of motion, the deeper the observed dark resonance. The curves plotted in figure 7 show the changing contrast in the observation of the dark resonance, as a function of modified compensation voltages applied on the correction electrodes. Depending on their distance from the center of the trap, a DC voltage applied on one of the correction electrodes moves the ion by about 100 to 400 nm per Volt. Variations of a tenth of a Volt have an impact on the micromotion and can be detected through the variation of the dark resonance contrast. In addition, we have made sure, that the applied static voltages do not modify the ion's position in the laser beams. The inset of figure 7 shows the contrast  $\mathcal{C}$  of the dark resonance versus the applied compensation voltage and a maximum can be unambiguously distinguished. We have verified that this maximum corresponds to a reduced spectral linewidth of the blue cooling transition. The blue linewidth represents an estimate of the ion's kinetic energy when approximated by a Doppler profile. It cannot be taken as an absolute measure as it depends strongly on the applied (blue) laser intensity, however it is a good relative indication of the kinetic energy state of the ion, when the Doppler broadening is larger than the power broadening. Compensation parameters have been tested on all four correction electrodes, resulting in the best localisation of a single ion.

### D. Laser beam geometry

Equation (8) shows that the dark resonance condition changes on the time scale of the oscillation period of the ion, which is at least two orders of magnitude smaller than the observation time. For fixed laser detunings, the Doppler shifts fulfill the dark resonance condition only for a fraction of the oscillation period, this fraction decreases with increasing velocity amplitude and with increasing wave vector difference  $\vec{k}_B - \vec{k}_R$ . In the case of a  $\text{Ca}^+$  ion  $|k_B| \approx$

$|2k_R|$ , we then expect the sensitivity to ion oscillation three times higher for the counterpropagating configuration than for the copropagating one (cf. figure 2).

This behaviour has been checked experimentally by using the alternative beam geometry where both lasers enter the trap from the same direction. In this configuration, dark resonances can be observed in almost any case, even with a small ion cloud, which is not possible in our experiment with the antiparallel geometry. As an example, figure 8 shows the fluorescence spectrum of three ions observed with copropagating laser beams.

To evidence the difference between co- and counterpropagating laser beam geometry we have plotted the highest dark resonance contrast  $\mathcal{C}$  as a function of the experimental linewidth of the  $4S_{1/2} - 4P_{1/2}$  transition in figure 9. Again, the measured fluorescence linewidth gives a relative indication of the degree of localisation of the trapped ion, as the smaller it is, the closer the ion is to the center of the trap. The general tendency of figure 9 is clearly visible: while dark resonances could not be observed at all for the counterpropagating geometry unless a certain level of localization has been reached, the copropagating geometry allows the observation of dark resonances for much hotter ions and even for small ion clouds. The highest contrast values achieved for counterpropagating laser beam geometry exceed 80%, reflecting an excellent localisation of the ion. In this beam configuration, the steeper slope in the variation of the contrast values as depicted in figure 9 can be used as a sensitive tool to reveal the degree of localization of the trapped ions with a high sensitivity.

## VI. CONCLUSION

In this paper we have presented a novel approach to reduce the micromotion of an ion confined in a miniature electrodynamic trap. Only the lasers for cooling and detection of the ion are necessary for the implementation of the proposed technique, in contrast to other techniques, in particular the probing of the vibrational sidebands which requires a highly stabilized laser to probe a narrow-linewidth transition. We use the contrast of the dark resonances observed with two counterpropagating laser beams to collect information about the motional state of the ion. Numerical simulations and experiments have shown that this contrast is very sensitive to the localisation of the ion, while a larger micromotion amplitude smears out the coherent population trapping effect. Observation of fluorescence is made on time bins which are long compared to the inverse motional frequencies of the ion. On this timescale, the oscillation amplitudes along the three directions are coupled in the trap.

Comparison with other compensation techniques is not straightforward as the different methods produce various signal levels and use different sets of experimental parameters. In any case, the maximum fluorescence signal has to be monitored as a function of the compensation voltages, to make sure that a decrease in the observed signal height is not due to the fact that the ion has been pushed out of the laser beams. The spatial displacement of the confined particle with lowered pseudo-potential well depth requires the use of a detector with spatial resolution and can only be applied to reduce effects which appear in the plane of observation. The exploration of the linewidth on the  $4S_{1/2} - 4P_{1/2}$ -transition is an easy method to roughly minimize excess micromotion, keeping in mind that the linewidth depends also on the applied laser intensities and frequencies which may modify the efficiency of laser cooling. Since excess micromotion may also deform the excitation spectrum of the ion, it is important to record the entire frequency response at fixed laser intensities. The fluorescence correlation method which shows the modulation of the ion's fluorescence with the micromotion frequency  $\Omega$  gives best signal-to-noise ratios in the low intensity limit but requires an integration time of at least a couple of seconds to accumulate sufficient signal in each time channel of a time-to-amplitude converter [11].

Due to the wide panel of recorded signals a quantitative comparison of the different compensation methods cannot be made in a precise way. As a matter of fact, best results for the reduction of excess micromotion are obtained by using at least two different methods. Measurements along multiple laser axes have to be performed to assure a complete extinction of excess micromotion for all projections in space. We have shown that even in the case where the blue laser linewidth is not modified, dark resonances can still be observed. It is thus possible to use this means of micromotion reduction, when the rf correlation technique and the observation of the blue transition linewidth fail. The main advantage of the dark resonance technique is nevertheless its simplicity and the absence of need for any other recording or excitation devices than those used for fluorescence observation.

In summary, we propose a complementary method to reduce excess micromotion of a single trapped ion making use only of the experimental means necessary to detect the ion's fluorescence. In a more general way, this technique

can be applied to any three-level ion having a  $\Lambda$  energy scheme, the highest sensitivity being reached for  $k_B = k_R$ .

- 
- [1] E. Arimondo. *Coherent Population Trapping in Laser Spectroscopy*, volume XXXV of *Progress in Optics*, chapter V, pages 258–354. E. Wolf, elsevier science b.v. edition, 1996.
- [2] C. F. Roos, D. Leibfried, A. Mundt, F. Schmidt-Kaler, J. Eschner, and R. Blatt. Experimental demonstration of ground state laser cooling with electromagnetically induced transparency. *Phys. Rev. Lett.*, 85:5547, 2000.
- [3] G. Morigi. Cooling atomic motion with quantum interferences. *Phys. Rev. A*, 67:033402, 2003.
- [4] G. Janik, W. Nagourney, and H. Dehmelt. Doppler-free optical spectroscopy on the  $\text{Ba}^+$  mono-ion oscillator. *J. Opt. Soc. Am. B*, 2:1251–1257, 1985.
- [5] Y. Stalgies, I. Siemers, B. Appasamy, T. Altevogt, and P. E. Toschek. The spectrum of single-atom resonance fluorescence. *Europhys. Lett.*, 35:259, 1996.
- [6] D. Reiss, K. Abich, W. Neuhauser, Ch. Wunderlich, and P.E. Toschek. Raman cooling and heating of two trapped  $\text{Ba}^+$  ions. *Phys. Rev. A*, 65:053401, 2002.
- [7] F. Kurth, T. Gudjons, B. Hilbert, T. Reisinger, G. Werth, and A.-M. Maartensson-Pendrill. Doppler free "dark resonances" for hyperfine measurements and isotope shifts in  $\text{Ca}^+$  isotopes in a paul trap. *Z. Phys. D.*, 34:227–232, 1995.
- [8] Patrick Gill. *Proceedings of the Sixth Symposium on Frequency Standards and Metrology*. World Scientific Ltd, Singapore, 2002.
- [9] R. H. Dicke. The effect of collisions upon the Doppler width of spectral lines. *Phys. Rev.*, 89:472, 1953.
- [10] B.E. King, C.J. Myatt, Q.A. Turchette, D. Leibfried, W.M. Itano, C. Monroe, and D.J. Wineland. Cooling the collective motion of trapped ions to initialize a quantum register. *Phys. Rev. Lett.*, 81:3631, 1998.
- [11] D.J. Berkeland, J.D. Miller, J.C. Bergquist, W.M. Itano, and D.J. Wineland. Minimization of ion micromotion in a Paul trap. *J. Appl. Phys.*, 83:5025, 1998.
- [12] M. Knoop, M. Vedel, and F. Vedel. Lifetime, collisional-quenching, and  $j$ -mixing measurements of the metastable  $3D$  levels of  $\text{Ca}^+$ . *Phys. Rev. A*, 52:3763, 1995.
- [13] J. Lidberg, A. Al-Khalili, L.-O. Norlin, P. Royen, X. Tordoir, and S. Mannervik. Lifetimes of the metastable  $3d^2d_{3/2}$  and  $3d^2d_{5/2}$  levels in  $\text{Ca}^+$  measured by laser probing of a stored ion beam. *J. Phys. B*, 32:757, 1999.
- [14] W. Paul. *Rev. Mod. Phys.*, 62:531, 1990.
- [15] F. Diedrich, J.C. Bergquist, W.I. Itano, and D.J. Wineland. Laser cooling to the zero-point energy of motion. *Phys. Rev. Lett.*, 62:403, 1989.
- [16] A. Aspect, E. Arimondo, R. Kaiser, N. Vansteenkiste, and C. Cohen-Tannoudji. Laser cooling below the one-photon recoil energy by velocity-selective coherent population trapping. *Phys. Rev. Lett.*, 61:826, 1988.
- [17] M. Schubert, I. Siemers, and R. Blatt. Line shape of three-level ions in paul traps. *Phys. Rev. A*, 39:5098, 1989.
- [18] H.G. Dehmelt. Radiofrequency spectroscopy of stored ions I: storage. *Advances in Atomic and Molecular Physics*, 3:53–72, 1967.
- [19] C. Champenois, M. Knoop, M. Herbane, M. Houssin, T. Kaing, M. Vedel, and F. Vedel. Characterization of a miniature Paul-Straubel trap. *Eur. Phys. J. D*, 15:105, 2001.
- [20] M. Knoop, C. Champenois, G. Hagel, M. Houssin, C. Lisowski, M. Vedel, and F. Vedel. Metastable level lifetimes from electron-shelving measurements with ion clouds and single ions. *Eur. Phys. J. D*, 29:163–171, 2004.



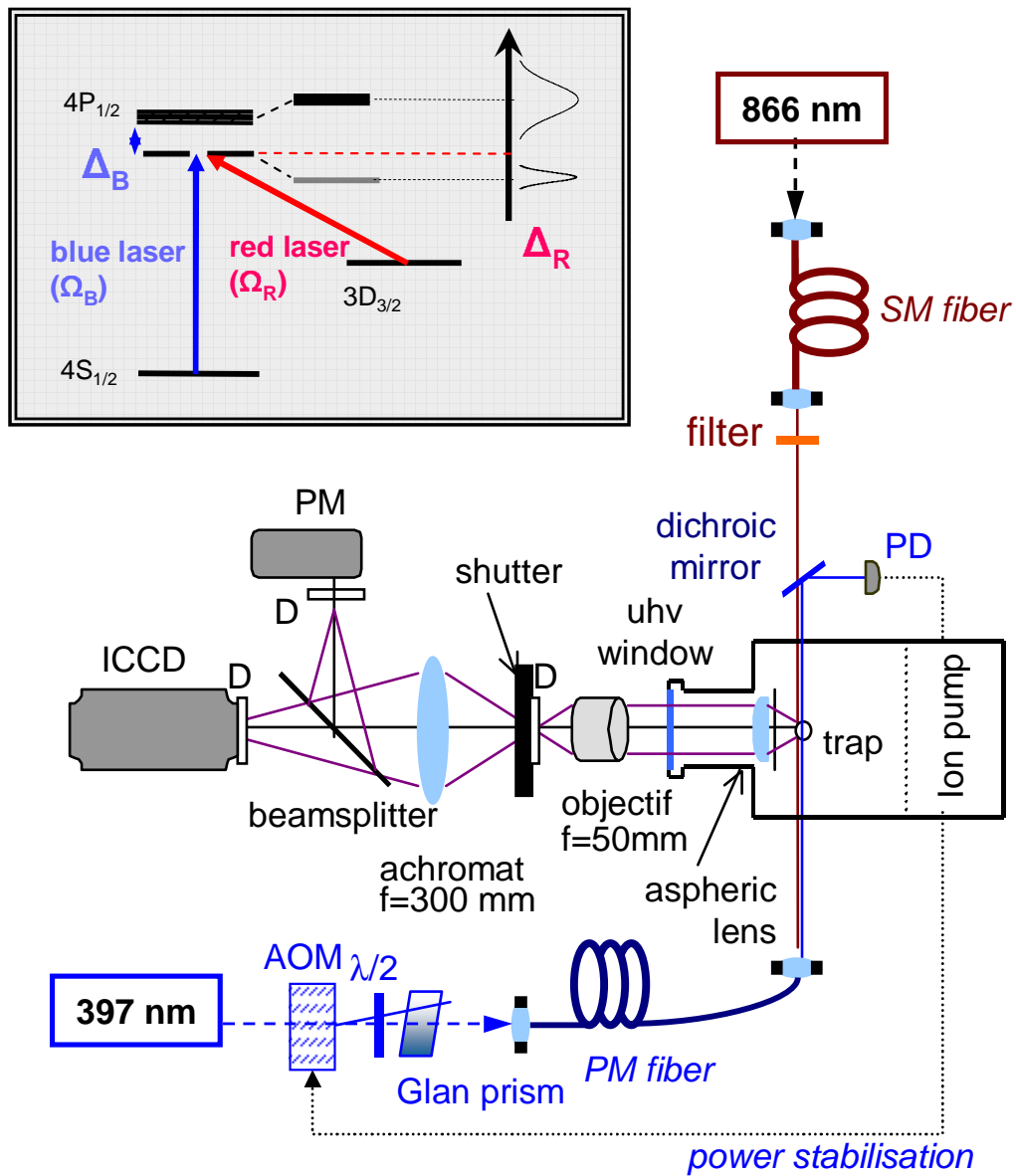


FIG. 1: Experimental setup with counterpropagating laser beams. The left-hand inset shows the first energy levels of a  $\text{Ca}^+$ -ion dressed by the blue photons.

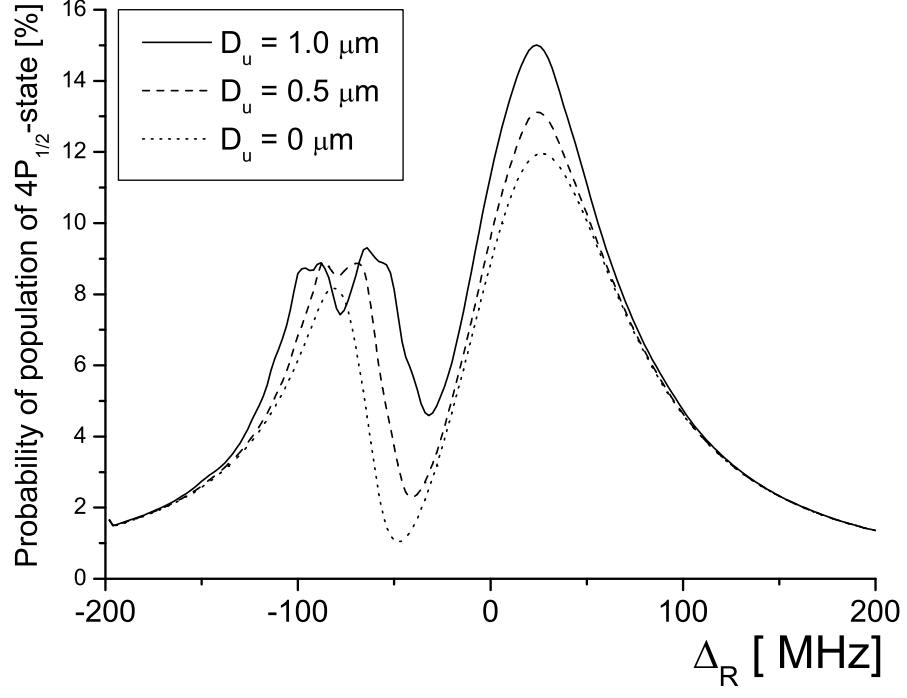


FIG. 2: Numerical simulation of dark resonances in the counter-propagating laser beam geometry, for a velocity amplitude  $V_0 = 1$  m/s and different displacements  $D_u$  off the trap center. ( $\Omega_B = 120$  MHz,  $\Omega_R = 30$  MHz,  $\Delta_B = -50$  MHz.)

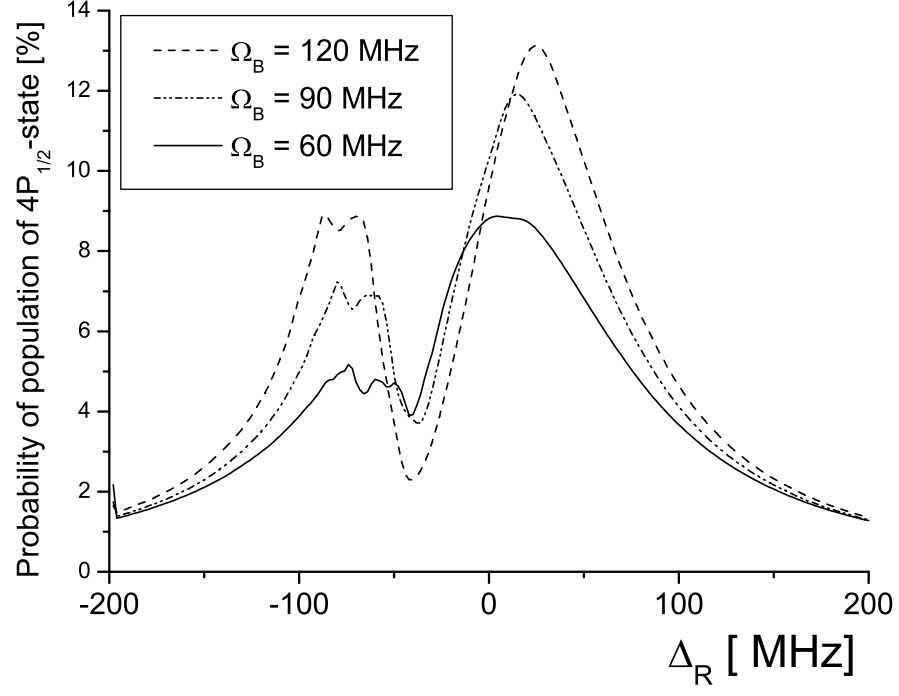


FIG. 3: Numerical simulation of the observable dark resonance signal for different blue Rabi frequencies  $\Omega_B$ . The two laser beams are counterpropagating and the motion of the ion is described by  $V_0 = 1$  m/s and  $D_u = 0.5$   $\mu\text{m}$ . Micromotion sidebands are visible in the spectrum at lower  $\Omega_B$ . ( $\Omega_R = 30$  MHz,  $\Delta_B = -50$  MHz.)

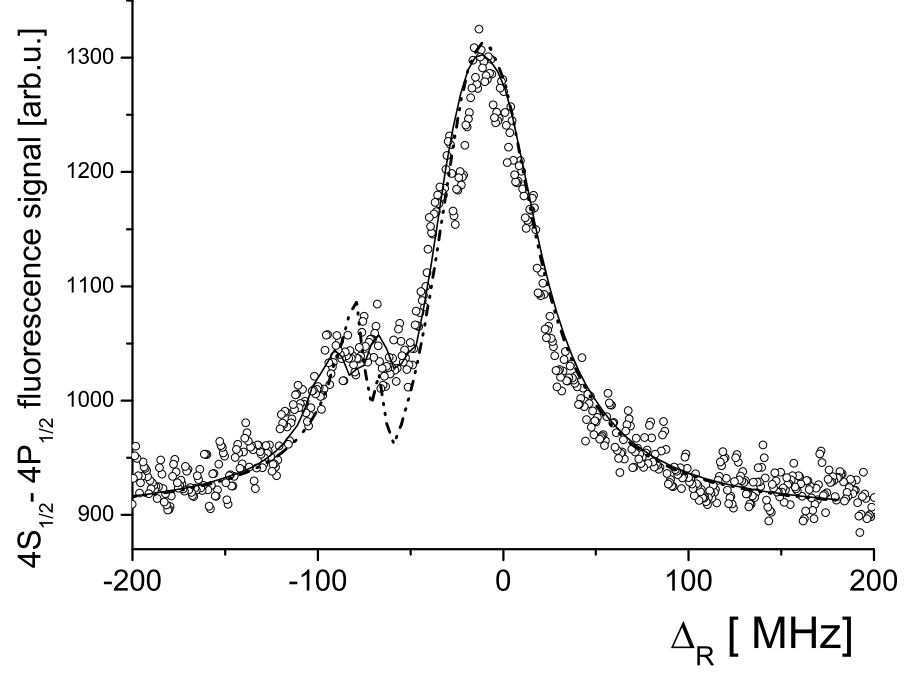


FIG. 4: Experimental observation of a dark resonance ( $\circ$ ), adjusted by the numerical simulation with counter-propagating laser beams (solid line). The dashed line is the numerical simulation with an identical parameter set and with co-propagating laser beams. ( $\Omega_B = 60$  MHz,  $\Omega_R = 15$  MHz,  $\Delta_B = -50$  MHz,  $V_0 = 1$  m/s, and  $D_u = 0.8$   $\mu\text{m}$ .)

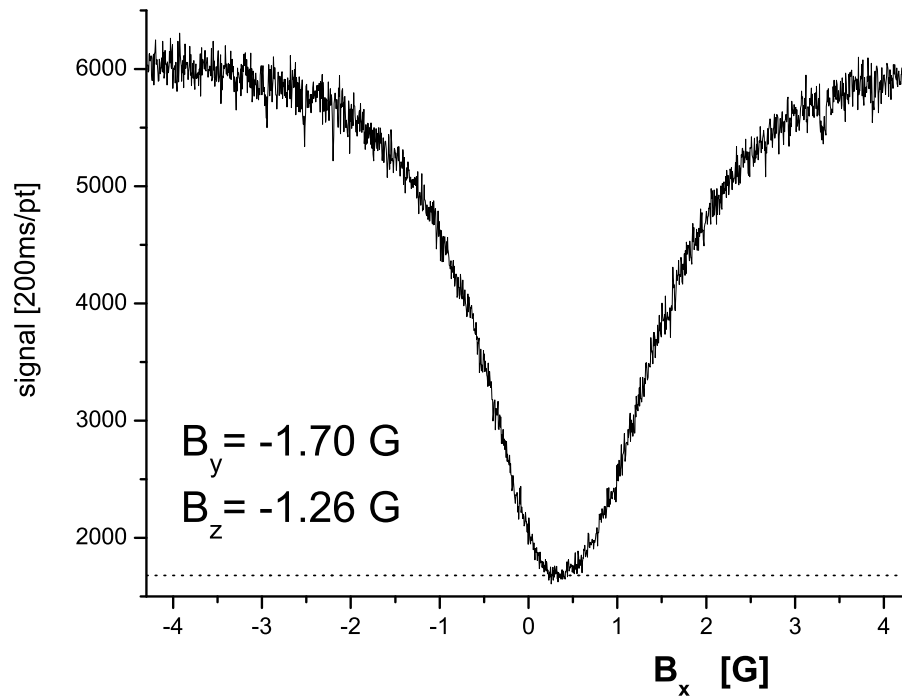


FIG. 5: Fluorescence of a single ion versus the applied perpendicular magnetic field in a Hanle type experiment for the determination of the magnetic field zero values. The red laser is linearly polarized along the  $x$  direction. The dotted line corresponds to the background light level.

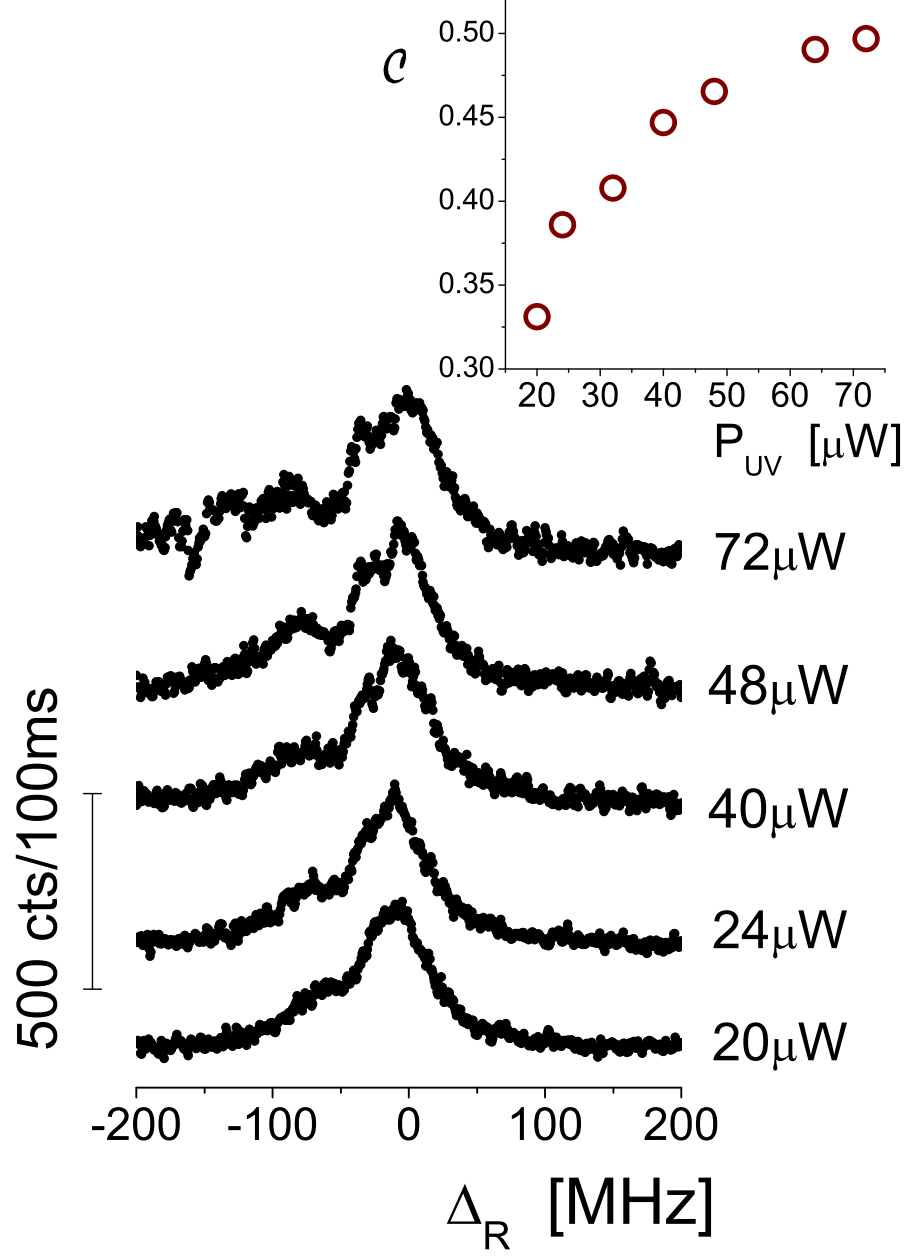


FIG. 6: Dark resonances observed with counterpropagating laser beams. The graph shows the influence of the laser power on the level splitting, the offset of the curves is due to the varying laser power. The applied blue laser powers are marked on the right-hand side of the curves, where the lowest value corresponds to about  $2 \Gamma_B$  while the highest power is equivalent to  $4 \Gamma_B$ . The inset shows the increasing contrast of the dark resonance with higher laser power.

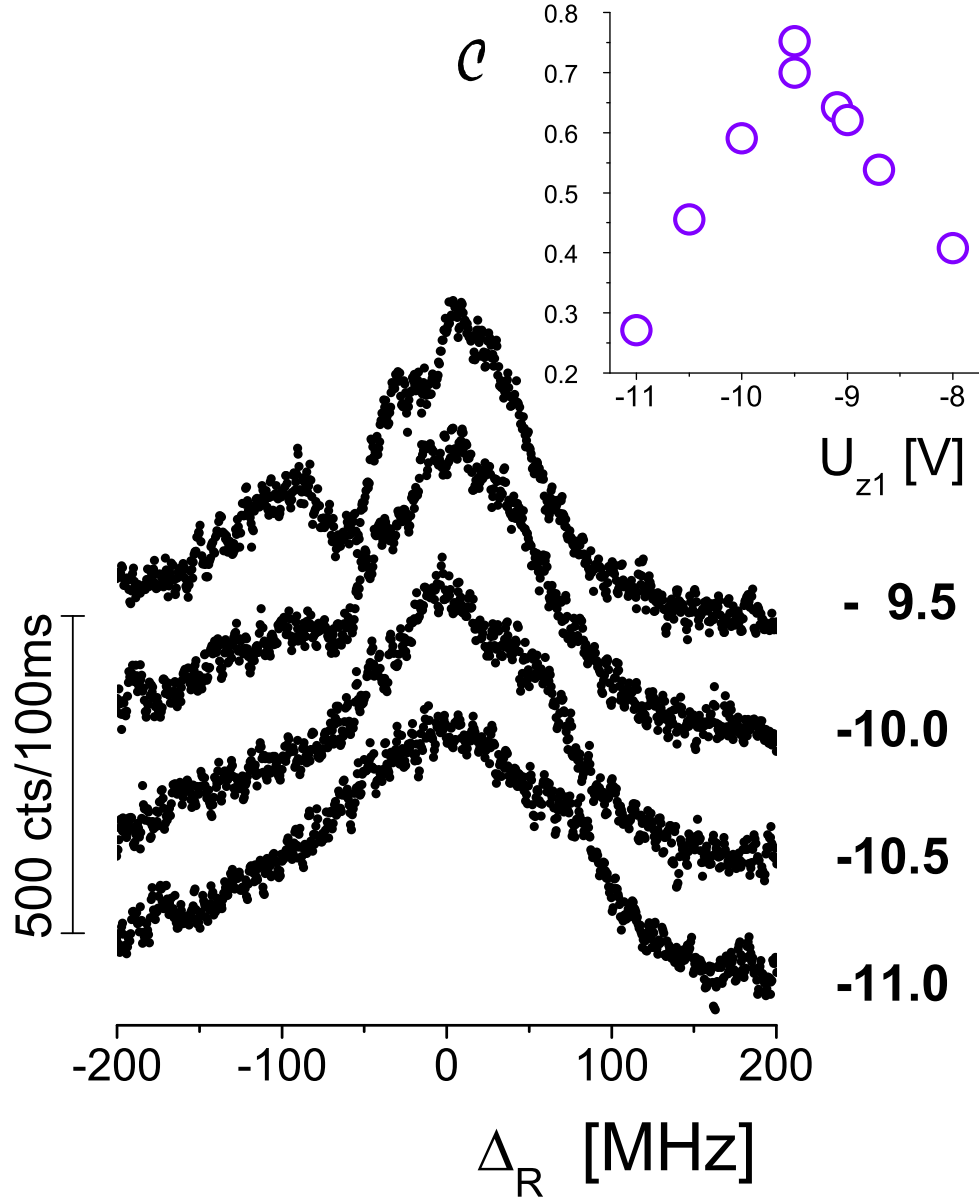


FIG. 7: Influence of the micromotion on the observed dark-resonance contrast  $\mathcal{C}$  with counterpropagating laser beams, laser intensity:  $\Omega_B \approx 4\Gamma_B$ ,  $\Omega_R \approx 10\Gamma_R$ . For better visibility, the graph only shows selected curves which have been offset by a fixed value. The compilation of the contrast data in the inset allows an unambiguous determination of the best compensation parameter.

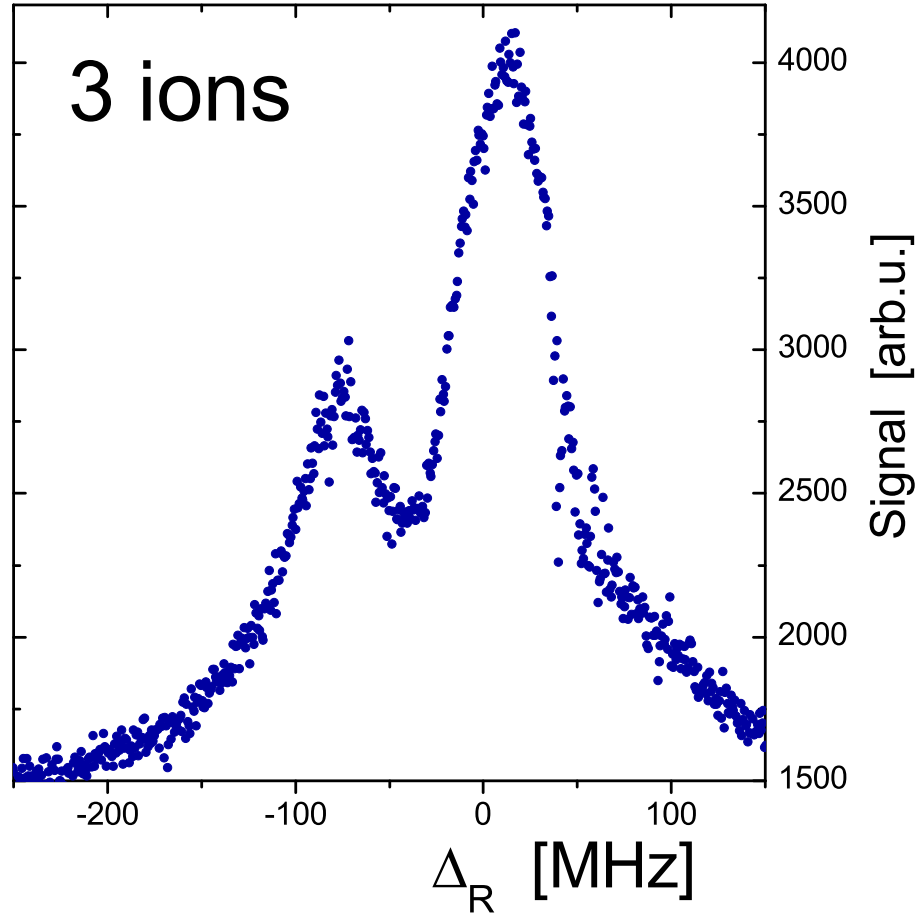


FIG. 8: Dark resonance observed in the fluorescence of a 3-ion cloud with copropagating laser beams.



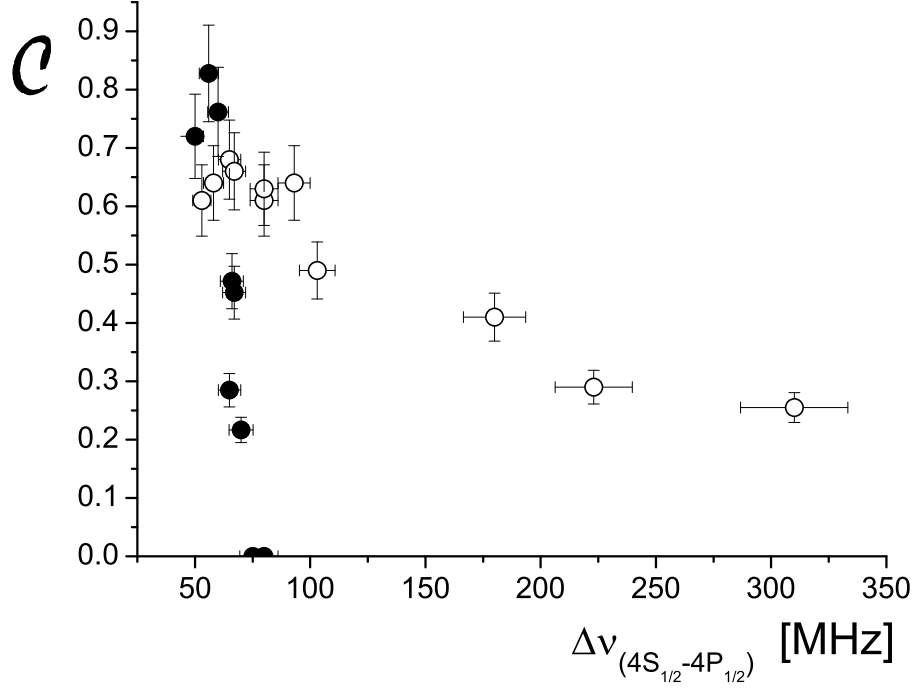


FIG. 9: Comparison of the dark resonance contrast for co- (○) and counter-propagating (●) laser beam geometry. In the graph the highest measured contrast is plotted as a function of the observed transition linewidth on the  $4S_{1/2}-4P_{1/2}$  transition. The data for the copropagating geometry has been taken with a single ion for linewidths below about 100 MHz, and with very small ion clouds (inferior to 10 particles) for linewidths above. For this experiment, the blue transition linewidths are due to micromotion and not to power broadening.